JBC RESEARCH ARTICLE

Vitamin D receptor inhibits EMT *via* regulation of the epithelial mitochondrial function in intestinal fibrosis

Received for publication, October 9, 2020, and in revised form, February 22, 2021 Published, Papers in Press, March 11, 2021, https://doi.org/10.1016/j.jbc.2021.100531

Mengli Yu[1,‡], Hao Wu[2,‡], Jinhai Wang[3,‡], Xueyang Chen[1], Jiaqi Pan[1], Peihao Liu[1], Jie Zhang[1], Yishu Chen[1], Wei Zhu[1], Chenxi Tang[1], Qi Jin[1], Chunxiao Li[4], Chao Lu[1], Hang Zeng[1], Chaohui Yu[1,*], and Jing Sun[5,*]

From the [1]Department of Gastroenterology, The First Affiliated Hospital, College of Medicine, Zhejiang University, Hangzhou, China; [2]Department of Gastroenterology and Hepatology, Zhongshan Hospital, Fudan University, Shanghai, China; [3]Department of Colorectal Surgery, The First Affiliated Hospital, College of Medicine, Zhejiang University, Hangzhou, China; [4]Department of Gastroenterology, Ningbo First Hospital, Ningbo, China; [5]Department of Gastroenterology, Ruijin Hospital, Shanghai Jiao Tong University School of Medicine, Shanghai, China

Edited by Dennis Voelker

We previously showed that the vitamin D receptor (VDR) plays a crucial role in acute inflammatory bowel disease and that intestinal fibrosis is a common complication of Crohn's disease (CD). Epithelial–mesenchymal transition (EMT) is an important hallmark of fibrogenesis through which epithelial cells lose their epithelial phenotype and transform into mesenchymal cells. It is known that the VDR plays an essential role in epithelial integrity and mitochondrial function, but its role in intestinal fibrosis remains unknown. Here, we investigated whether the VDR is involved in epithelial mitochondrial dysfunction that results in EMT in intestinal fibrosis. Using human CD samples, intestine-specific VDR-KO mice, and fibroblast cellular models, we showed that the expression of the VDR was significantly lower in intestinal stenotic areas than in nonstenotic areas in patients with chronic CD. Genetic deletion of the VDR in the intestinal epithelium exacerbated intestinal fibrosis in mice administered with dextran sulfate sodium or 2,4,6-trinitrobenzene sulfonic acid, two experimental colitis inducers. In addition, we found that vitamin D dietary intervention regulated intestinal fibrosis by modulating the intestinal expression of the VDR. Mechanistically, knocking down the VDR in both CCD-18Co cells and human primary colonic fibroblasts promoted fibroblast activation, whereas VDR overexpression or VDR agonist administration inhibited fibroblast activation. Further analysis illustrated that the VDR inhibited EMT in the HT29 cell model and that mitochondrial dysfunction mediated epithelial integrity and barrier function in VDR-deficient epithelial cells. Together, our data for the first time demonstrate that VDR activation alleviates intestinal fibrosis by inhibiting fibroblast activation and epithelial mitochondria-mediated EMT.

Intestinal fibrosis is a common complication of Crohn's disease (CD), and the underlying mechanism has not been fully clarified (1). Repeated episodes of inflammation cause extracellular matrix (ECM) deposition in the mucosa and submucosa, and patients with CD gradually develop intestinal fibrosis (2). As reported, 30% to 50% of patients with CD develop intestinal fibrosis, which is characterized by lumen stenosis and complicated by fistulas and local abscesses, within 10 years (3, 4). In addition, except for surgical resection, there is no effective way to eliminate symptoms, and the recurrence rate after surgery is as high as 55% to 70% within 10 years (5). Although fibrosis is caused by repeated episodes of inflammation, controlling CD activity alone cannot prevent or reverse intestinal fibrosis (6). Therefore, it is vital to elucidate the pathological mechanism and explore potential targets for the intervention and treatment of intestinal fibrosis.

Luminal narrowing and obstruction, which are evident in the intestinal fibrotic process, are characterized by excessive accumulation of ECM components (7). ECM deposition mainly results from the activation of myofibroblasts, which originate from resident mesenchymal cells (8, 9). In addition to the ECM, activated myofibroblasts produce type I and III collagens, mucopolysaccharides, remodeling enzymes such as matrix metalloproteinases (MMPs), and profibrotic cytokines such as transforming growth factor-β1 (TGF-β1) (10). In chronic dextran sulfate sodium (DSS)-induced murine colitis, profibrotic genes such as alpha smooth muscle actin (α-SMA), Collagen I, MMP-9, and connective tissue growth factor (CTGF) (11) are abundantly activated, and activated myofibroblasts originate from various sources during fibrogenesis (12, 13). In addition, epithelial–mesenchymal transition (EMT) is an important hallmark of fibrogenesis (14), through which epithelial cells lose their polarized epithelial phenotype and transform into mesenchymal cells, including myofibroblasts (13, 15). As reported, sustained TGF-β1 upregulation was found in the intestinal fibrotic areas of patients with CD with elevated levels of EMT-related transcription factors (15). However, the mechanism of EMT in the pathogenesis of intestinal stricture is not fully understood.

The vitamin D receptor (VDR) is a member of the steroid receptor family and a vital regulator of skeletal health and

‡ These authors share the first authorship.
* For correspondence: Chaohui Yu, zyyyych@zju.edu.cn; Jing Sun, sunjingrj@shsmu.edu.cn.

calcium and phosphorus homeostasis (16). The VDR forms a VDR–retinoid X receptor heterodimeric complex and then binds to specific DNA sequences after being activated by $1,25(OH)_2D_3$ (17). The inhibitory effects of vitamin D (VD) and the VDR on acute colitis have been reported previously (18–20), but the potential effect of the VDR on intestinal fibrosis is currently poorly understood. Previous studies reported diminished VDR protein levels in the intestines of patients with CD compared with control tissues (21). In addition, a VD-deficient diet downregulated VDR expression and promoted chronic 2,4,6-trinitrobenzene sulfonic acid (TNBS)-induced intestinal fibrosis (22). Knocking down the VDR facilitated the expression of α-SMA and collagen I in colonic subepithelial myofibroblasts through the TGF-β1/Smad3 pathway (22). Based on this evidence, we hypothesized that the VDR might have an inhibitory effect on intestinal fibrosis.

The VDR plays an essential role in the mitochondrial respiratory process (23). As reported, the VDR has an essential biosynthetic function in the mitochondrial respiratory chain activity and facilitates the energy-producing tricarboxylic acid cycle during cellular proliferation (23). In a human epidermal keratinocyte cell line, VDR ablation increased the production of reactive oxygen species (ROS), resulting in cellular damage, the loss of mitochondrial integrity, and even apoptotic death in a long-term observation study (24). In contrast, VD treatment inhibited oxidative stress and mitochondrial dynamics in C2C12 muscle cells (25). However, there are currently no reports about VDR-mediated regulation of mitochondrial function in CD-induced intestinal fibrosis. Given these results, we hypothesized that the VDR was a vital modulator of intestinal fibrosis by regulating mitochondrial functions.

The aim of this study was to investigate the effect of the VDR on the pathogenesis of intestinal fibrosis. To this end, we established two classic mouse models of intestinal fibrosis: intestinal epithelium–specific VDR KO and VD dietary intervention. In addition, we used CCD-18Co and human primary colonic fibroblasts to examine the effect of the VDR on fibroblast activation and HT29 cells to explore potential EMT mechanisms. Furthermore, CD intestinal tissues were collected to verify clinical significance. We hypothesized that in the absence of the VDR, fibroblasts could be activated, during which mitochondrial dysfunction would occur in the epithelium, disrupt barrier integrity, and consequently promote EMT and ECM deposition. This mitochondria-dependent VDR/EMT pathway suggests a previously unrecognized mechanism of intestinal fibrogenesis and a novel strategy for antifibrotic therapies.

Results

VDR expression was decreased in the stenotic colonic tissues of patients with chronic CD and intestinal fibrosis mouse models

To examine the role of the VDR in intestinal fibrosis, we obtained colonic tissues from both stenotic areas and nonstenotic control areas from the same patients with CD. H&E staining revealed significant broadening of the mucosa, submucosa, and even muscularis in stenotic areas compared with nonstenotic areas (Fig. 1*A*). Quantification of Masson's trichrome staining showed massive collagen deposition in the submucosa and mucosa of stenotic areas (Fig. 1, *A* and *B*). Strikingly, quantitative PCR analysis of colonic tissues from patients with CD showed increased expression of various fibrosis markers in stenotic areas, including a myofibroblast marker (α-SMA), ECM markers (fibronectin, type I collagen, and CTGF), and MMP-2 and MMP-9 (Fig. 1*C*). In CD colonic tissues, downregulation of the VDR in stenotic areas was observed, as indicated by immunohistochemistry (IHC) staining, and these results were further confirmed at the mRNA and protein levels (Fig. 1, *D*–*F*). In addition, in intestinal fibrosis mouse models, VDR expression was dramatically decreased in the intestines in both chronic DSS–induced mice and chronic TNBS–induced mice (Fig. 1, *G* and *H*). Thus, our data indicated enhanced ECM deposition in fibrotic intestinal tissues, accompanied by a significant decrease in VDR expression.

Genetic deletion of the VDR in the intestinal epithelium exacerbated intestinal fibrosis in mice

To further explore the specific role of the intestinal VDR in the pathogenesis of intestinal fibrosis, we generated intestine-specific VDR-KO ($VDR^{IEC\text{-}KO}$) mice, and their littermate $VDR^{fl/fl}$ mice (flox) were used as controls (Fig. S1*A*). Repetitive administration of 2% DSS was used to mimic CD-induced intestinal fibrosis. In $VDR^{IEC\text{-}KO}$ mice, complete knockdown of VDR expression in colon tissues was confirmed at both the mRNA and protein levels (Fig. 2, *D* and *E*). During DSS administration, $VDR^{IEC\text{-}KO}$ mice showed a significantly higher body weight loss than $VDR^{fl/fl}$ mice beginning on day 36 (Fig. 2*A*). In addition, the $VDR^{IEC\text{-}KO}$ group was more sensitive to DSS administration, as indicated by a higher death rate and more severe colonic obstruction than those of the $VDR^{fl/fl}$ control group (Fig. S1, *B* and *D*), although the colon lengths were similar in the two groups (Fig. S2*C*). In addition, epithelium-specific knockdown of the VDR increased collagen deposition (Fig. 2*B*) and resulted in higher fibrosis and inflammation scores (Fig. 2*C*). Quantitative PCR analysis of the colonic tissues of DSS-induced mice revealed increased expression of fibrosis markers, including fibronectin, MMP-9 and TIMP-1, and inflammation markers, including interleukin-6 and chemokine (C-X-C motif) ligand (Fig. 2*F*). Although collagen I, TGF-β1, and MMP-2 only showed an increasing trend after chronic DSS administration, these factors were significantly increased in DSS-induced $VDR^{IEC\text{-}KO}$ mice compared with mice in the $VDR^{fl/fl}$ DSS group (Fig. 2*F*, Fig. S1*E*). In addition, Western blot analysis confirmed the activation of the classic TGF-β1 signaling pathway and ECM deposition, especially in $VDR^{IEC\text{-}KO}$ DSS mice (Fig. 2*F*). These findings suggested that VDR KO in the intestinal epithelium exacerbated chronic DSS-induced intestinal fibrosis and inflammation in mice.

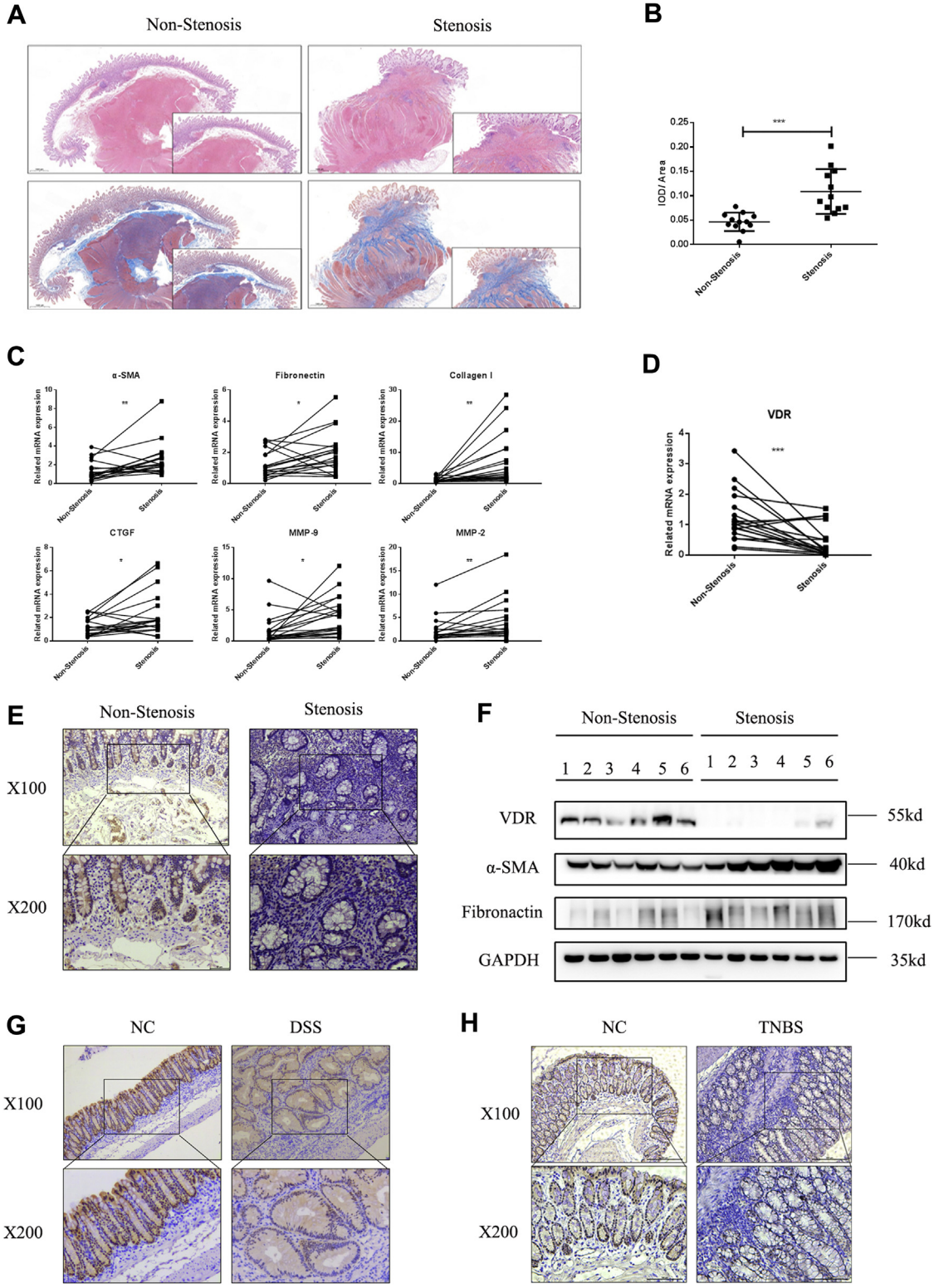

Figure 1. VDR was decreased in the stenotic colonic tissues of patients with chronic CD and intestinal fibrosis model mice. *A*, representative H&E staining and Masson's trichrome staining of colon sections from nonstenotic controls and stenotic areas of the same patients with CD are shown. The *scale bars* represent 1 mm. *B*, quantification of collagen deposition was measured in three representative areas per sample (stenotic n = 12, nonstenotic n = 12). Quantitative data are shown as the mean values with SD and differences (***$p < 0.001$, two-tailed). *C*, qPCR analysis of colonic tissues taken from stenotic and nonstenotic areas of patients with CD (n = 19 paired samples) by using paired *t* tests (*$p < 0.05$, **$p < 0.01$, two-tailed). *D*, representative images of IHC analysis of VDR are shown. The *scale bars* represent *upper* 100 μm and *lower* 50 μm. *E*, VDR expression was quantified by qPCR in stenotic and nonstenotic areas of patients with CD (n = 19 paired samples) by using paired *t* tests (***$p < 0.001$, two-tailed). *F*, representative Western blot images of VDR, α-SMA, and fibronectin expression (n = 6 paired samples). *G*, IHC staining of the VDR in the intestines of chronic DSS model mice. *Upper*, 100×; *lower*, 200×. *H*, IHC staining of the VDR in the intestines of chronic TNBS model mice. *Upper*, 100×; *lower*, 200×. α-SMA, alpha smooth muscle actin; CD, Crohn's disease; DSS, dextran sulfate sodium; IHC, immunohistochemistry; TNBS, 2,4,6-trinitrobenzene sulfonic acid; VDR, vitamin D receptor.

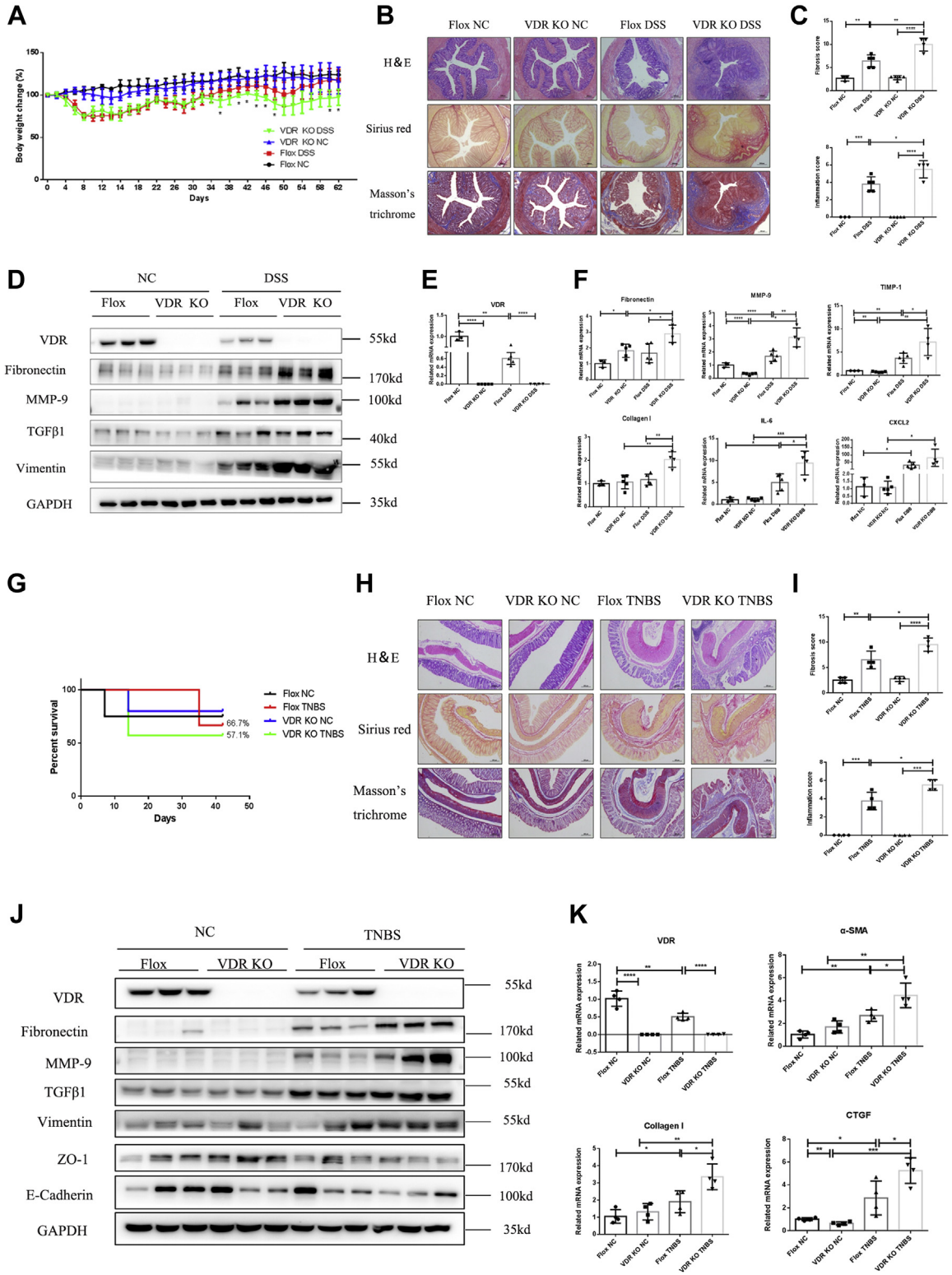

Figure 2. VDR-specific KO in the intestinal epithelium exacerbated intestinal fibrosis in mice. *A*, changes in the body weight percent (Flox NC n = 3, Flox DSS n = 5, VDR KO NC n = 5, VDR KO DSS n = 4 [*$p < 0.05$, two-tailed, Flox DSS *versus* VDR KO DSS]). *B*, representative H&E staining, Sirius red staining, and Masson's trichrome staining of colon sections. The *scale bars* represent 200 μm. *C*, quantification of the histological inflammation and fibrosis scores (*$p < 0.05$, **$p < 0.01$, ***$p < 0.001$, two-tailed). *D*, Western blot analysis of colon tissues from representative samples in each group (n = 3). *E*, VDR expression in the murine colon was measured by quantitative PCR (**$p < 0.01$, ****$p < 0.0001$, two-tailed). *F*, quantification of gene expression (*$p < 0.05$, **$p < 0.01$, ***$p < 0.001$, two-tailed). *G*, survival rates of TNBS-induced intestinal fibrosis model mice. *H*, H&E staining, Sirius red staining, and Masson's trichrome staining of colon sections. Representative images are shown. The *scale bars* represent 200 μm. *I*, quantification of the inflammation score and fibrosis score (Flox NC n = 4; Flox TNBS n = 4; VDR KO NC n = 4; VDR KO TNBS n = 4; *$p < 0.05$, **$p < 0.01$, ***$p < 0.001$, ****$p < 0.0001$, two-tailed). *J*, Western blot analysis of representative samples in each group (n = 3). *K*, quantitative PCR analysis of colon tissues (*$p < 0.05$, **$p < 0.01$, ***$p < 0.001$, ****$p < 0.0001$, two-tailed). DSS, dextran sulfate sodium; TNBS, 2,4,6-trinitrobenzene sulfonic acid; VDR, vitamin D receptor.

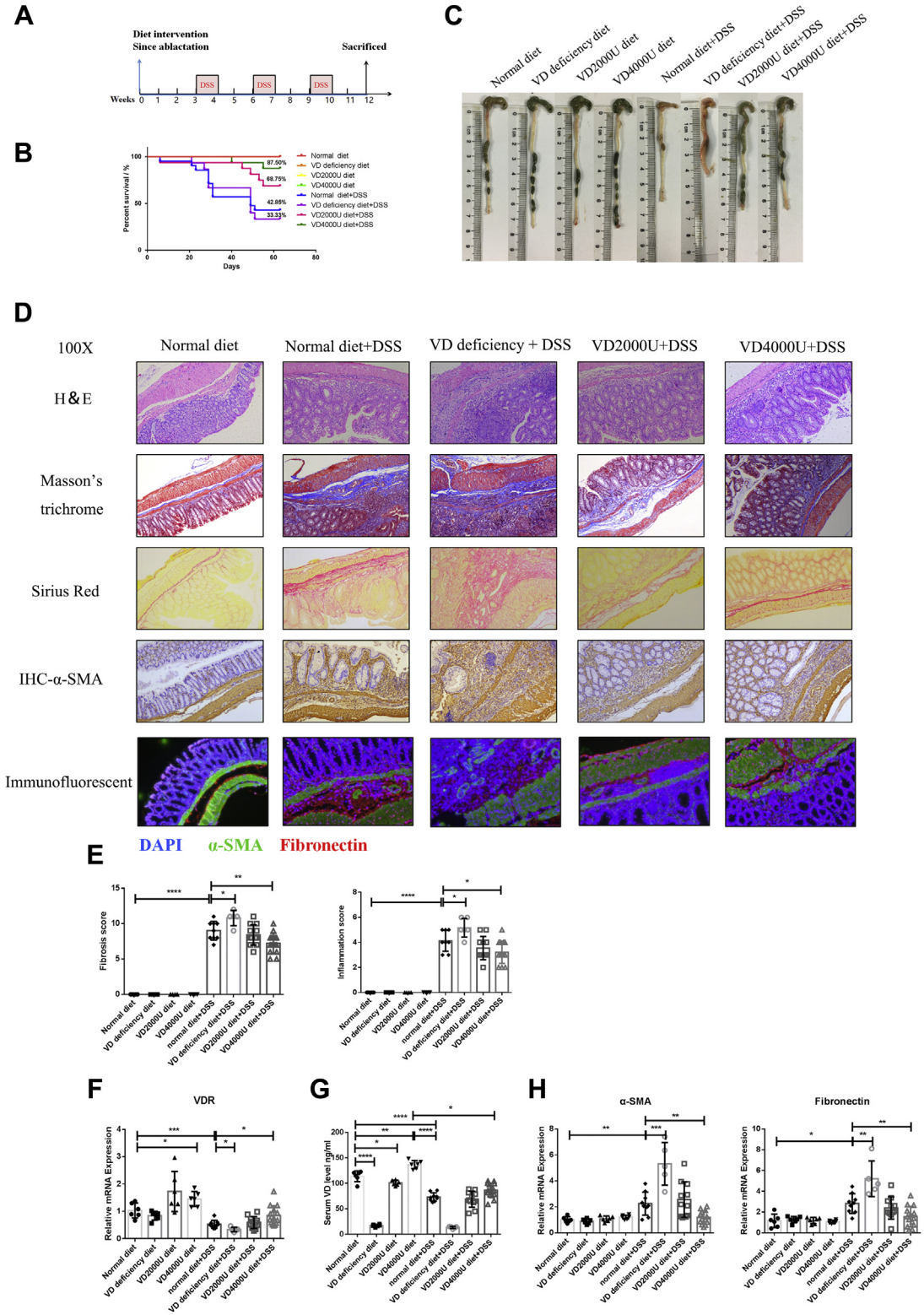

Figure 3. VD dietary intervention regulated the development of DSS-induced intestinal fibrosis in mice. *A*, the timeframe of the VD dietary intervention experiment. *B*, the percent survival rate in the VD dietary intervention experiment. *C*, representative images of mouse colons. *D*, representative H&E staining, Sirius red staining, Masson's trichrome staining, α-SMA IHC staining, and immunofluorescence staining of mouse colon sections. Magnification: 100×. *E*, quantification of histological inflammation and fibrosis scores (normal diet n = 6, VD-deficient diet n = 6, VD2000U diet n = 6, VD4000U diet n = 6, normal diet + DSS n = 9, VD-deficient diet + DSS n = 5, VD2000U diet + DSS n = 11, VD4000U diet + DSS n = 14, $*p < 0.05$, $**p < 0.01$, $****p < 0.0001$, two-tailed). *F*, VDR gene expression at the RNA level ($**p < 0.01$, $****p < 0.0001$, two-tailed). *G*, serum levels of VD ($*p < 0.05$, $**p < 0.01$, $****p < 0.0001$, two-tailed). *H*, quantification of gene expression ($*p < 0.05$, $**p < 0.01$, $***p < 0.001$, two-tailed). α-SMA, alpha smooth muscle actin; DSS, dextran sulfate sodium; IHC, immunohistochemistry; VD, vitamin D; VDR, vitamin D receptor.

As TNBS administration is a well-recognized approach to mimic colitis induced by the immune response, we verified the effect of the VDR on chronic TNBS-induced intestinal fibrosis. Repetitive administration of TNBS caused high death rates. The survival rate of the VDR^{IEC-KO} TNBS group was 57.1%, while that of the $VDR^{fl/fl}$ TNBS group was 66.7% (Fig. 2*G*). The colon lengths in the two TNBS groups were not different (Fig. S1*F*). In addition, treatment with TNBS in epithelium-specific VDR-knockdown mice resulted in an histological grade and exacerbated intestinal inflammation and ECM deposition (Fig. 2, *H* and *I*). Chronic TNBS administration caused a dramatic decrease in VDR expression (Fig. 2, *J* and *K*). Western blot analysis revealed that VDR KO in the epithelium increased the expression of fibronectin, MMP-9, and TGF-β1 after 6 weeks of TNBS administration (Fig. 3*J*). The increased mRNA levels of these genes also indicated that the VDR KO was an exacerbating factor in TNBS-induced fibrosis (Fig. 2*K*, Fig. S1*G*). In addition, we found that vimentin expression was increased, accompanied by decreased expression of zonulin-1 (ZO-1) and E-cadherin, which indicated increased activation of the EMT process in VDR^{IEC-KO} TNBS mice (Fig. 3*J*). These results showed that the intestinal epithelium–specific VDR KO exacerbated TNBS-induced intestinal fibrosis and EMT.

VD dietary intervention regulated the development of DSS-induced intestinal fibrosis in mice

Previous studies reported that repeated TNBS administration increased intestinal inflammation and fibrosis in mice fed a VD-deficient diet, whereas a VD-sufficient diet alleviated fibrosis by inhibiting TGF-β1/Smad3 signal transduction (22). However, the effect VD dietary intervention on chronic DSS-induced fibrosis mouse models is unknown, considering the different pathogeneses associated with TNBS and DSS administration. Thus, we investigated the effect of VD intervention on intestinal fibrosis. Male C57BL/6 mice were given a VD-deficient diet or VD-supplemented diet before 3 weeks of repeated DSS administration (Fig. 3*A*). DSS administration induced obvious body weight loss, especially in the VD-deficient group (Fig. S2*A*). The survival rate of the VD-deficient DSS group was only 33.3%, while that of the VD-supplemented DSS group, especially the VD4000U group, increased to 87.5% (Fig. 3*B*). In addition, morphologically, the VD-deficient group showed worsened hematochezia, edema, and stiffness, although there was no statistically significant difference in the colon length between the DSS groups (Fig. 3*C*, Fig. S2*B*). Feeding DSS-induced mice a VD-deficient diet exacerbated chronic inflammation and fibrosis (Fig. 3, *D* and *E*), whereas in the VD-supplemented group, fibrosis and inflammation were highly improved compared with those in the normal-diet group (Fig. 3, *D* and *E*). In addition, tissue IHC staining and immunofluorescence staining revealed that the VD-deficient diet increased ECM deposition and fibroblast activation, whereas the VD-supplemented diet showed inhibitory effects (Fig. 3*D*). Furthermore, VD dietary intervention modulated the serum levels of VD and influenced the expression of the VDR in intestinal tissues (Fig. 3, *F* and *G*). The mRNA levels of α-SMA and fibronectin also indicated that the VD-deficient diet exacerbated DSS-induced fibrosis and chronic inflammation, whereas the VD4000U supplementary diet alleviated symptoms (Fig. 3*H*, Fig. S2*C*). Therefore, VD dietary intervention regulated the development of intestinal fibrosis by modulating the intestinal expression of the VDR.

VDR inhibited fibroblast activation in vitro

Intestinal fibrosis is characterized by abnormal tissue repair and the massive deposition of ECM proteins, which are produced by activated myofibroblasts (26). To investigate the effect of the VDR on the activation of fibroblasts, we purchased human colon fibroblasts (CCD-18Co cells) from the American Type Culture Collection and purified and cultured primary human intestinal fibroblasts. First, we used VD to activate VDR signaling and mimic the biological functions of VD (Fig. 4*C*; Fig. S3, *A* and *B*). We found an increase in the number of α-SMA–positive CCD-18Co cells after treatment with TGF-β1 for 48 h (Fig. 4*A*). The number of α-SMA–positive cells was decreased in the VD pretreatment group (Fig. 4*A*). At the transcriptional level, VD pretreatment significantly decreased α-SMA expression after CCD-18Co cells were activated with TGF-β1 (Fig. 4*B*). In primary human intestinal fibroblasts, VD dramatically decreased the expression of α-SMA and fibronectin, which were stimulated by TGF-β1 (Fig. 4*C*). Then, we used calcitriol to pharmacologically activate the VDR. In CCD-18Co cells, although calcitriol could slightly increase the expression of the VDR, fibronectin and CTGF were decreased by calcitriol treatment (Fig. S3*C*). Flow cytometric analysis showed that the fibroblast activation marker α-SMA was significantly decreased by calcitriol in the presence of TGF-β1 (Fig. 4*D*). In primary human intestinal fibroblasts, calcitriol significantly increased the expression of the VDR and dramatically decreased α-SMA and fibronectin expression in the presence of TGF-β1 stimulation (Fig. 4, *E* and *F*). Furthermore, VDR overexpression by Flag-tagged VDR plasmid transfection significantly increased VDR expression and alleviated α-SMA expression in CCD-18Co cells (Fig. 4*G*, Fig. S3*D*). In addition, VDR overexpression inhibited fibrosis markers induced by TGF-β1 stimulation in primary human intestinal fibroblasts, including α-SMA, fibronectin, CTGF, MMP-9, and TGF-β/Smad pathway factors (Fig. 4, *H* and *I*). Moreover, we identified the VDR exerted its effects in the presence of the VD ligand (Fig. S3*E*). Therefore, pharmacological stimulation of the VDR and overexpression of the VDR both inhibited the increase in fibrosis markers and fibroblast activation.

These results indicated that the VDR gene had an inhibitory effect on fibroblast activation. A loss-of-function experiment was performed for further investigation. We found that siRNA-mediated knockdown of the VDR significantly exacerbated TGF-β1-induced fibroblast activation and ECM deposition in primary human intestinal fibroblasts

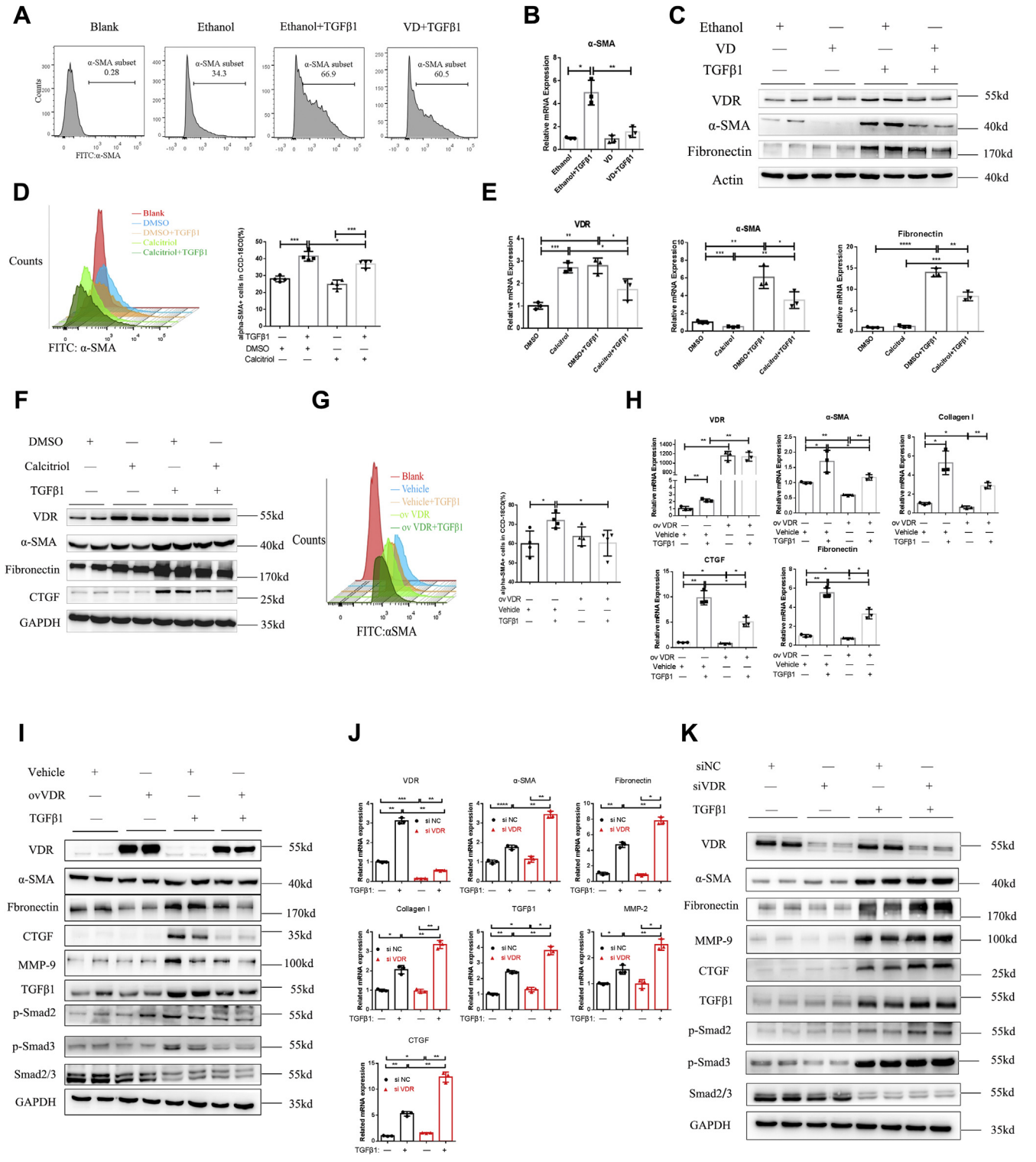

Figure 4. VDR modulated fibroblast activation *in vitro*. *A*, FACS analysis of α-SMA-positive CCD-18Co cells and the percentage of α-SMA-positive cells (%). *B*, quantitative PCR analysis of α-SMA expression in CCD-18Co cells (n = 3, $*p < 0.05$, $**p < 0.01$, two-tailed). *C*, Western blot analysis of primary human intestinal fibroblasts after pretreatment with VD or ethanol for 12 h and TGF-β1 stimulation for another 48 h. *D*, FACS analysis of α-SMA-positive CCD-18Co cells treated with calcitriol (10 nm) and TGF-β1 for 48 h and quantification of α-SMA-positive CCD-18Co cells (n = 4, $*p < 0.05$, $***p < 0.001$, two-tailed). *E*, quantitative PCR analysis of α-SMA and fibronectin expression in primary human intestinal fibroblasts (n = 3, $*p < 0.05$, $**p < 0.01$, $***p < 0.001$, $****p < 0.0001$, two-tailed). *F*, Western blot analysis of primary human intestinal fibroblasts. *G*, FACS analysis of CCD-18Co cells and quantification of α-SMA-positive cells (n = 4, $*p < 0.05$, two-tailed). VDR overexpression by Flag-tagged VDR plasmid transfection and TGF-β1 administration for 48 h. *H*, Western blot analysis of fibrosis pathways in VDR-overexpressing primary human intestinal fibroblasts. *I*, gene expression in primary human intestinal fibroblasts was measured by quantitative PCR (n = 3, $*p < 0.05$ $**p < 0.01$, two-tailed). *J*, quantitative PCR analysis of fibrosis-related genes in primary human intestinal fibroblasts (n = 3, $*p < 0.05$, $**p < 0.01$, $***p < 0.001$, $****p < 0.0001$, two-tailed). *K*, Western blot analysis of primary human intestinal fibroblasts transfected with siRNA and stimulated with TGF-β1 for 48 h. α-SMA, alpha smooth muscle actin; FACS, fluorescence activated cell sorting; TGF-β1, transforming growth factor-β1; VDR, vitamin D receptor.

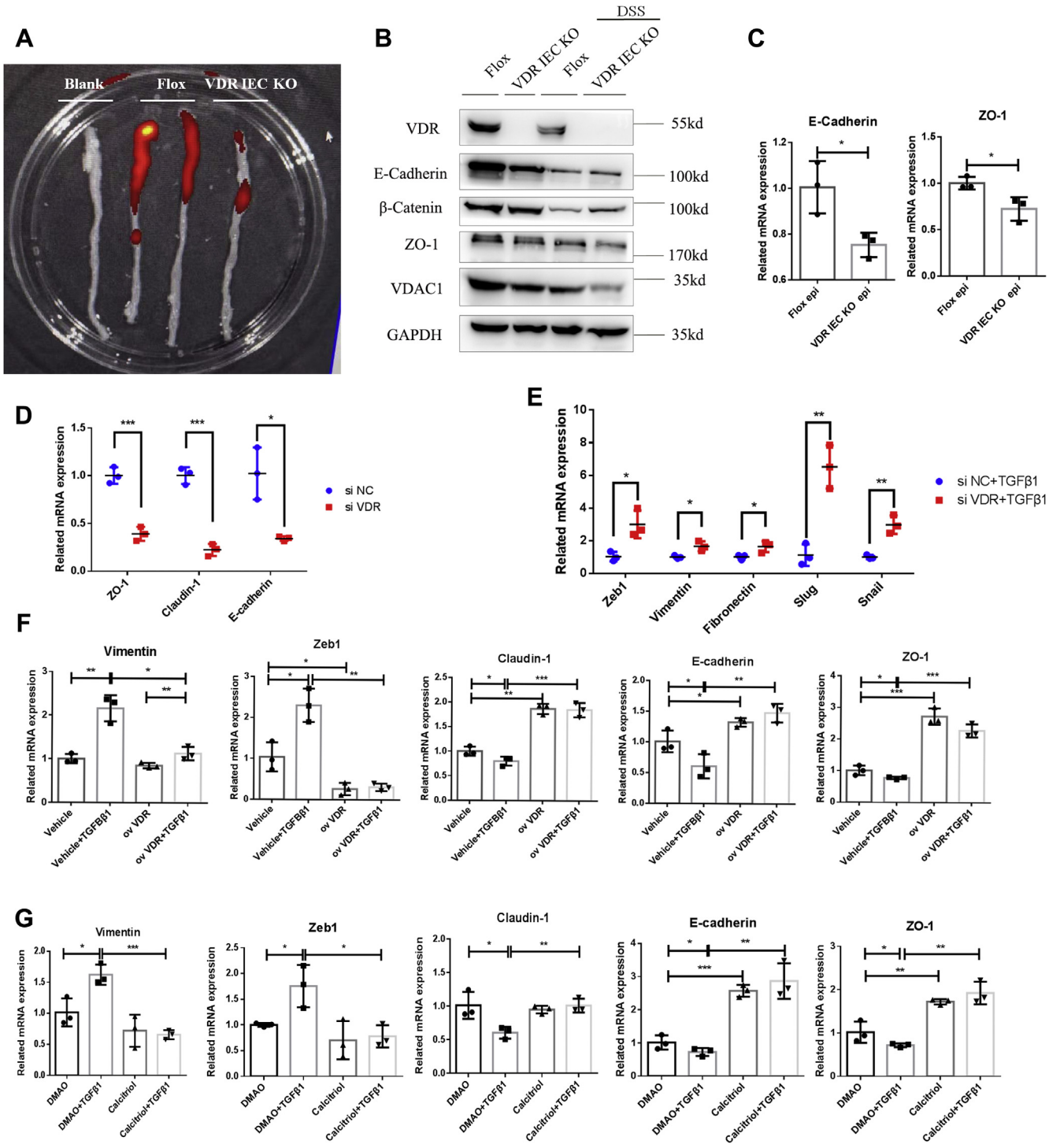

Figure 5. VDR mediated epithelial integrity and inhibited intestinal fibrosis through EMT. *A*, the image of mouse colons at 6 h after gavage. *B*, Western blot analysis of isolated mouse epithelial tissues. *C*, qPCR analysis of isolated mouse epithelial tissues (n = 3, $*p < 0.05$, two-tailed). *D*, qPCR analysis of epithelial markers in VDR-knockdown HT29 cells (n = 3, $*p < 0.05$, $**p < 0.01$, two-tailed). *E*, qPCR analysis of mesenchymal markers in TGF-β1-induced and VDR-knockdown HT29 cells (n = 3). *F*, VDR overexpression was induced by Flag-tagged VDR plasmid transfection and TGF-β1 administration in HT29 cells, and gene expression was measured by quantitative PCR (n = 3, $*p < 0.05$, $**p < 0.01$, $***p < 0.001$, two-tailed). *G*, TH-29 cells were treated with calcitriol (10 nm) and TGF-β1 for 5 days, and gene expression was measured by quantitative PCR (n = 3, $*p < 0.05$, $**p < 0.01$, $***p < 0.001$, two-tailed). EMT, epithelial–mesenchymal transition; TGF-β1, transforming growth factor-β1; VDR, vitamin D receptor.

(Fig. 4, *J* and *K*). Furthermore, TGF-β1 expression was increased in the VDR-knockdown group, combined with the upregulation of p-smad2 and p-smad3, suggesting activated TGF-β1–Smad signaling in VDR-deficient fibroblasts (Fig. 4*K*). Therefore, activated fibroblasts promoted intestinal fibrosis. Taken together, these findings indicated that

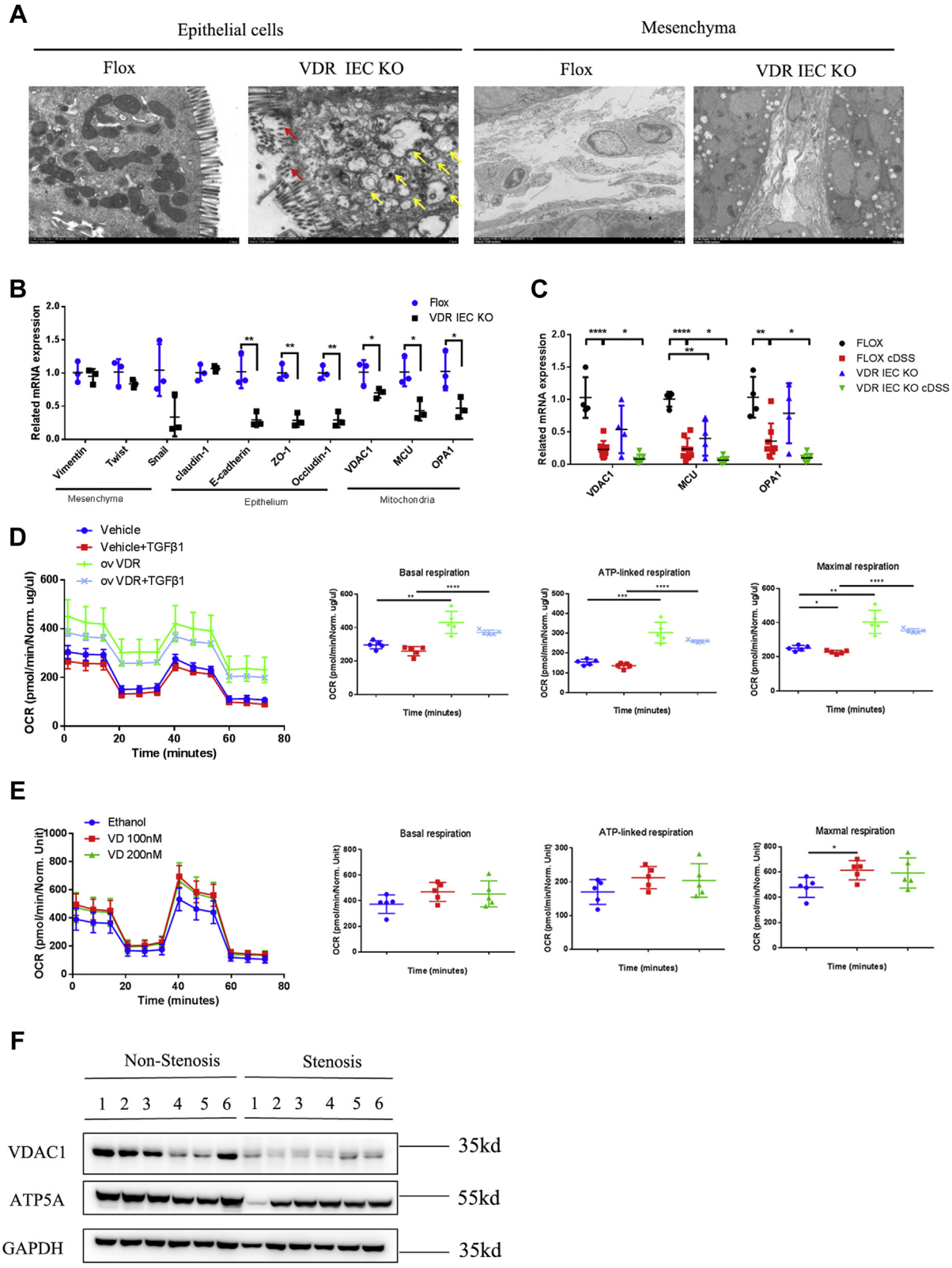

Figure 6. VDR deficiency caused mitochondrial dysfunction in intestinal epithelial cells. *A*, mitochondrial morphology was observed by electron microscopy. *Yellow arrows*, mitochondrial swelling and vesicular formation. *Red arrows*, damaged villi of intestinal epithelial cells. (epithelial cell magnification: 7000×, the *scale bars* represent 2 μm; mesenchymal cell magnification: 15,000×; the *scale bars* represent 10 μm). *B*, qPCR analysis of isolated mouse epithelial tissues (n = 3, $*p < 0.05$, $**p < 0.01$, two-tailed). *C*, gene expression in mouse colons was measured by quantitative PCR (Flox NC n = 3; Flox DSS n = 5; VDR KO NC n = 5; VDR KO DSS n = 4; $*p < 0.05$, $**p < 0.01$, $****p < 0.0001$, two-tailed). *D*, HT29 cells were infected with virus containing an overexpression vector for the VDR or an empty vector. The concentrations of FCCP, oligomycin, and rotenone/antimycin A were 1.5 μM, 0.5 μM, and 0.5 μM, respectively. Each measurement was performed five times and normalized to the protein content of the cells ($*p < 0.05$, $**p < 0.01$, $***p < 0.001$, $****p < 0.0001$, two-tailed). *E*, the OCR of HT29 cells in response to 10 nm and 20 nm VD or ethanol for 24 h (n = 5, $*p < 0.05$ two-tailed). *F*, representative Western blot images of mitochondrial functional gene expression (n = 6 paired samples). DSS, dextran sulfate sodium; FCCP, carbonyl cyanide-4 (trifluoromethoxy) phenylhydrazone; OCR, oxygen consumption rate; VDR, vitamin D receptor.

knocking down the VDR exacerbated primary human intestinal fibroblast activation.

VDR deficiency impaired epithelial integrity and promoted intestinal fibrosis by upregulating the EMT pathway

As reported, the gut epithelial VDR inhibited colitis by protecting the mucosal epithelial barrier and maintaining mucosal integrity (19, 20), although only a few studies illustrated the mechanism of this protective effect against colitis. Here, we found that VDR KO in the intestinal epithelium suppressed mucosal absorptive function *in vivo* (Fig. 5*A*). We isolated epithelial layers from both VDR-KO mice and control mice after repeated DSS administration. We found that the expression levels of E-cadherin, ZO-1, and β-catenin, the most representative markers of the epithelial barrier function, were significantly decreased in VDR-KO mice, especially after DSS administration (Fig. 5, *B* and *C*). Considering that the downregulation of epithelial markers is related to EMT, which is one of the main sources of mesenchymal fibroblasts, EMT was promoted in VDR-KO mice. In addition, the expression levels of epithelial markers, including E-cadherin, ZO-1, and β-catenin, were significantly decreased in mice with DSS-induced chronic intestinal fibrosis, whereas the expression levels of mesenchymal markers, including vimentin and Slug, were increased, indicating that EMT is a vital process in intestinal fibrosis (Fig. S4, *A* and *B*). Therefore, we further explored the relationship between intestinal epithelial VDR expression and EMT in fibrosis.

We evaluated the effects of the VDR gene on the human intestinal epithelial tumor cell line HT29 by establishing a well-characterized model of TGF-β1-induced EMT (27, 28). In HT29 cells, knockdown of VDR expression decreased epithelial integrity (Fig. 5*D*; Fig. S5*A*). When we activated EMT by administering TGF-β1 to HT29 cells, mesenchymal markers were dramatically elevated in the VDR-deficient group (Fig. 5*E*). In addition, VDR overexpression significantly alleviated the expression of Vimentin and Zeb1, while elevating the expression of epithelial markers such as E-cadherin, ZO-1, and claudin-1 (Fig. 5*F*; Fig. S5*B*). Similar results were observed after the pharmacological stimulation of the VDR (Fig. 5*G*; Fig. S5*C*). Taken together, these results indicated that the VDR could mediate epithelial integrity and inhibit intestinal fibrosis through modulating EMT.

Mitochondrial dysfunction mediated epithelial integrity in VDR-deficient epithelial cells

Mitochondrial morphological changes were analyzed by electron microscopy. We found that the intestinal epithelial cells in $VDR^{IEC\text{-}KO}$ mice exhibited mitochondrial swelling, vesicular formation, and villus disruption compared with those of $VDR^{fl/fl}$ mice (Fig. 6*A*). In addition, in the intestinal mesenchyme of $VDR^{IEC\text{-}KO}$ mice, the ECM greatly accumulated in the cellular interstices (Fig. 6*A*). We also measured mitochondrial functional genes to determine whether mitochondrial morphological changes were related to mitochondrial biogenesis. In epithelial cells isolated from $VDR^{IEC\text{-}KO}$ mice, the expression levels of epithelial connexins, as well as voltage-dependent anion-selective channel 1 (VDAC1), OPA1, and mitochondrial calcium uniporter (MCU), were greatly decreased (Fig. 6*B*). Coincidentally, chronic DSS administration also decreased the expression of the abovementioned mitochondrial functional genes (Fig. S6*A*). Therefore, we measured the expression of mitochondrial functional genes in chronic DSS-induced VDR-KO mice. We found that the expression levels of VDAC1, MCU, and OPA1 were significantly decreased in $VDR^{IEC\text{-}KO}$ DSS mice compared with $VDR^{fl/fl}$ DSS mice (Fig. 6*C*). Repeated TNBS administration showed little influence on VDR-regulated mitochondrial function (Fig. S6*B*). We also analyzed the cellular mitochondrial oxygen consumption rate (OCR) *in vitro*. In HT29 cells, VDR overexpression dramatically increased cellular basal respiration compared with that of the vehicle control (Fig. 6*D*). VDR overexpression significantly elevated ATP-coupled oxygen consumption and the maximal respiration rate (Fig. 6*D*). In addition, moderate VD administration increased maximal respiration in HT29 cells (Fig. 6*E*). These data suggested that the VDR elevated oxygen utilization for ATP production, enabling increased mitochondrial respiration, especially maximal respiration, in intestinal epithelial cells. Furthermore, in the colonic tissues of patients with CD, the downregulation of VDAC1 and ATP5A in stenotic areas indicated decreased numbers of mitochondria and cellular metabolic capacity (Fig. 6*F*). In conclusion, VDR deficiency in the gut impaired epithelial integrity and exacerbated intestinal fibrosis by promoting EMT and fibroblast activation.

In brief, the VDR inhibited intestinal fibrosis by regulating fibroblast activation and EMT (Fig. 7). On the one hand, the VDR inhibited the TGF-β/Smad pathway and prevented quiescent fibroblasts from differentiating into myofibroblasts, expressing α-SMA and secreting ECM. On the other hand, the VDR promoted epithelial integrity

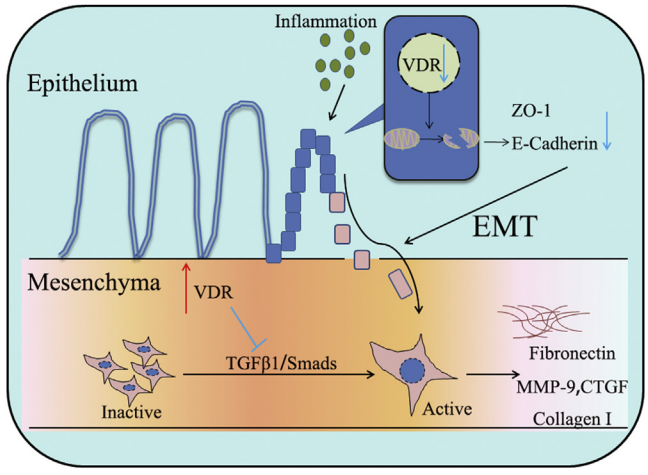

Figure 7. Summary of the pathological and underlying mechanisms by which the VDR inhibits intestinal fibrosis through EMT and fibroblast activation. EMT, epithelial–mesenchymal transition; VDR, vitamin D receptor.

and barrier function by maintaining the quality and number of mitochondria, thus decreasing inflammation-induced EMT.

Discussion

In this study, we aimed to investigate the effects of intestinal VDR expression on intestinal fibrosis. The results showed that VDR expression in the intestinal stricture tissues of patients with CD was significantly lower than that in nonstenotic tissues, and the downregulation VDR expression was observed in two different intestinal fibrosis mouse models. In support of our initial hypothesis, we found that epithelial-specific KO of the VDR promoted intestinal fibrosis in mice, while VD dietary intervention regulated the development of intestinal fibrosis by modulating intestinal VDR expression. In addition, activation of the VDR by VD, calcitriol, or VDR plasmids inhibited the expression of profibrotic factors in both CCD-18Co and human primary intestinal fibroblast models. In contrast, knocking down the VDR promoted profibrotic factors. In addition to the direct effect of VDR deficiency on fibroblasts, VDR deficiency in epithelial cells promoted EMT-related intestinal fibrosis in our study. We observed that VDR deficiency led to mitochondrial dysfunction in epithelial cells, indicating decreased energy production in epithelial cells, barrier integrity disruption, and the development of epithelial cell transformation. To our knowledge, we are the first to investigate the effect of the VDR on epithelial mitochondrial function and EMT-related intestinal fibrosis.

The VDR plays a protective role by exerting antifibrotic effects. In carbon tetrachloride–induced liver fibrosis, VDR activation in hepatic stellate cells suppresses liver inflammation and fibrosis (29). In addition, mice with VDR KO spontaneously develop hepatic fibrosis as a consequence of intersecting VDR/Smad genomic pathways (30). In acute enteritis, the VDR maintains intestinal epithelial integrity by inhibiting apoptosis and necroptosis (31, 32). Therefore, we investigated whether the VDR functions in intestinal fibrosis induced by repeated inflammation. In our study, we found that the VDR inhibited the activation of fibroblasts *in vitro* in both the human colonic fibroblast CCD-18Co cell line and human primary intestinal fibroblasts. During this process, the VDR significantly decreased the expression of the fibroblast marker α-SMA and ECM components, including fibronectin and collagen I. In addition, the VDR had an inhibitory effect on the phosphorylation of Smad2/3, which is a classic downstream molecule of TGF-β1. To verify the effects of the VDR on intestinal epithelia in EMT-related fibrosis, we established intestinal fibrosis models with intestinal epithelium–specific VDR-KO mice (20) and littermate controls. Mice with epithelial VDR deficiency developed worsened intestinal fibrosis in both the chronic TNBS and DSS models, followed by exacerbated EMT and mitochondrial dysfunction. Taken together, these results support the hypothesis that the VDR is crucial for fibroblast activation and EMT in intestinal fibrosis.

To mechanistically verify the contribution of the VDR to intestinal fibrosis, we examined the relationship between epithelial barrier integrity and EMT. As reported, EMT is an important mechanism that is responsible for the abnormal deposition of the ECM, resulting in the loss of the epithelial cell-to-cell basement membrane and generating a fibroblastic phenotype (33). The transformation of normal mammary epithelial cells can be mediated by VDR expression in tumorigenesis, indicating that the loss of the VDR promotes negative regulation of epithelial characteristics (34). In our EMT-related *in vitro* experiment, we found that the overexpression of the VDR or calcitriol treatment inhibited TGF-β1-induced EMT, which mainly manifested as decreased expression of the mesenchymal marker vimentin and elevated expression of epithelial junction proteins, including claudin, E-cadherin, and ZO-1. In contrast, VDR knockdown decreased epithelial markers and increased the EMT-related nuclear translocation of Zeb1, Slug, and Snail. However, the mechanism by which the VDR downregulates intestinal fibrosis through the EMT remains unclear. We hypothesized that VDR deficiency might induce damage to the epithelial barrier function, leading to epithelial cell transformation *via* the EMT process.

Mitochondria are vital organelles in intestinal epithelial cell energy metabolism. Previous studies reported that the VDR exerted beneficial effects on mitochondrial function in kidney fibrosis (35) and 1α,25(OH)2D3-mediated mitochondrial energy conversion (36) and maintained normal mitochondrial morphology (25) by regulating fission and fusion processes (37). The disruption of mitochondrial integrity and quality can be monitored by mitochondrial proteins such as VDAC1 (38, 39), MCU (40), and OPA1 (41). To prevent cell death, VDAC1 (42) and OPA1 (43) are involved in protecting against cytochrome C release and ROS production, thus maintaining the mitochondrial number and function. Collectively, the expression levels of these proteins represent mitochondrial integrity and quality. In our study, electron microscopy showed significant differences in mitochondrial morphological changes between the $VDR^{IEC\text{-}KO}$ and $VDR^{fl/fl}$ groups. Consistently, the OCR results verified that VDR overexpression increased the respiration rate and energy production, indicating the upregulation of mitochondrial integrity and quality. In addition, in the DSS-induced fibrosis model, VDR KO and DSS administration both decreased the expression of mitochondrial proteins, such as VDAC1, MCU, and OPA1, and $VDR^{IEC\text{-}KO}$ mice showed worsened mitochondrial functions. In conclusion, our study confirmed that the VDR could regulate the mitochondrial function in gut epithelial cells and inhibit EMT in intestinal fibrosis.

To verify the clinical value of the VDR in inhibiting intestinal fibrosis, we collected 19 samples of intestinal tissues from patients with CD and observed that the VDR was significantly decreased in stenotic areas compared with the corresponding nonstenotic areas. Previous studies reported that the VDR was reduced in fibroblasts isolated from the damaged tissues of patients with CD, and treatment with VD prevented migration and fibrosis in heterotopic transplanted colonic tissues (21), indicating the antifibrotic therapeutic value of VD. In addition, it was reported that VDR agonists

attenuated EMT by inhibiting the TGF-β1/Smad pathway (44), and E-cadherin expression was increased in response to VD treatment (45). Consistently, we found that the VDR inhibited fibroblast activation. In addition, the expression of VDAC1 and the ATP synthase–related protein ATP5A was much higher in stenotic areas than in nonstenotic areas, indicating mitochondrial dysfunction in stenotic epithelial areas. Therefore, our findings illustrated that VDR expression was closely related to intestinal epithelial mitochondrial function, which might be a new target for the prevention and treatment of intestinal fibrosis.

There are still some limitations in our study. Based on our present findings, further studies are needed to clarify the mechanisms by which the VDR regulates mitochondrial function. Here, we raised several hypotheses to explain the potential mechanism. As reported, the interaction of ECM molecule perlecan and dystroglycan was required for maintenance of the epithelial cell polarity (46), which may be the reason that mitochondria dysfunctional epithelial cells were tend to occur in the EMT process. Besides, we found that the VDR inhibited intestinal fibrosis under the regulation of SQSTM1/p62, which was reported a negative regulator of liver inflammation and fibrosis (29). SQSTM1/p62 was decreased in stenotic areas (Fig. S7*A*) and it inhibited fibroblasts activation *in vitro* (Fig. S7*B*). Coimmunoprecipitation and immunofluorescence staining showed that the VDR had direct interaction with SQSTM1/p62 (Fig. S7, *C* and *D*). Thus, SQSTM1/p62 is the possible upstream of the VDR, which regulates mitochondrial function and fibrosis, and further study about SQSTM1/p62 and VDR will be adopted. As for the potential downstream, some studies have indicated that the VDR modulates the mitochondrial function by regulating ROS production or through classic pathways, such as AMPK/SIRT1 and PI3K/Akt, in other organs (25, 36, 47, 48). Thus, broader mechanism researches on the VDR and epithelial mitochondrial function are needed in the future. In addition, both DSS- and TNBS-induced intestinal fibrosis mouse models showed high mortality, which was mainly caused by dehydration due to excessive inflammation in the early stage or intestinal obstruction in the later stage, leading to fewer model individuals. In addition, *in vitro* experiments showed significantly increased expression of the VDR in response to TGF-β1 administration, while the positive effects of the VDR on fibrosis were significant and consistent. A potential explanation for this effect is the positive feedback regulation of the VDR under TGF-β1 stimulation in fibroblasts. Although evidence showed the unliganded VDR worked in some situations (49), our study revealed the VDR had a fibrosis inhibitory effect in the presence of ligand *in vitro* (data not shown). Besides, we assumed the hedgehog pathway might be the downstream of the VDR (49, 50), while the underlying mechanism was still unclear in intestinal fibrosis. Further study about the liganded VDR and hedgehog pathway is expected.

In conclusion, our study showed that the VDR significantly alleviated CD-induced intestinal fibrosis by inhibiting fibroblast activation, maintaining epithelial mitochondrial function, and alleviating the EMT process, suggesting a key role of this protein in positively regulating intestinal fibrosis.

Experimental procedures

Human tissue samples

Intestinal tissue samples were obtained from patients with CD (n = 19) who underwent surgical resection of the intestine and were defined as stenotic/nonstenotic areas. The characteristics of the patients and normal subjects are summarized in Table S1. Paraffin-embedded intestinal sections were obtained from matched stenotic areas and nonstenotic areas of the same patient. For protein and RNA examination, tissues were separated from the intestines and immediately placed into liquid nitrogen for quick freezing and stored at −80 °C. Chronic CD was diagnosed by clinical symptoms, endoscopic examination, and pathological evaluations. This study was approved by the Ethics Committee of the First Affiliated Hospital, College of Medicine, Zhejiang University, Hangzhou, China.

Isolation and culture of primary human intestinal fibroblasts

Primary human intestinal fibroblasts were prepared according to the method reported by Scheibe *et al.* (51). Briefly, intestinal tissues were stored in the culture medium at 4 °C after being obtained from surgical patients, and cells were isolated as soon as possible. Intestinal tissues were washed with cold, sterile PBS at least 5 times. Then, the tissues were shaken and digested with an enzyme mix containing DNase I (1 mg/ml), collagenase D (1.5 mg/ml), and Dispase II (1.5 mg/ml) for 1 h at 37 °C in the medium until the tissue was fully dissolved (Roche). The digestion suspension was filtered with a 70-μm cell filter. Then, the cell suspension was centrifuged and resuspended in Dulbecco's modified Eagle's medium (DMEM)/Ham' F 12 (Invitrogen) containing 10% fetal bovine serum (Invitrogen) and 100 U/ml penicillin–streptomycin (Sigma-Aldrich), and 1.0×10^6 cells were plated in a 10-cm dish. The cultured medium was changed after 24 h. Analyses were performed on primary human intestinal fibroblasts at passages 3 to 8. Before stimulation, 3.0×10^5 cells were plated in a 6-cm dish.

Cell culture

The human intestinal myofibroblast cell line CCD-18Co was purchased from the American Type Culture Collection and was used as an *in vitro* intestinal myofibroblast cell model (52). HT29 cells were purchased from the Chinese Academy of Sciences. To develop an *in vitro* model to investigate EMT, HT29 cells were stimulated with TGF-β1 (10 ng/ml) for 7 days, and the medium was changed every 2 days. CCD-18Co and HT29 cells were both cultured in DMEM (Invitrogen) containing 10% fetal bovine serum and 100 U/ml penicillin–streptomycin at 37 °C in a humidified 5% CO_2 atmosphere.

To establish a fibroblast activation model, CCD-18Co cells and primary human intestinal fibroblasts were treated with recombinant human TGF-β1 (PeproTech) (10 ng/ml) for 48 h.

For VDR agonist experiments, cells were treated with 10-nM calcitriol (Selleck) or 100-μM VD (Sigma-Aldrich) for 12 h, and TGF-β1 (10 ng/ml) was added and incubated for another 48 h. In the VDR-knockdown experiment, primary human intestinal fibroblasts and HT29 cells were transfected with VDR-specific siRNAs (5'-GCAACCAAGACTACAAGTA-3') (Ribobio) or the corresponding negative control by Lipofectamine 3000 (Invitrogen). A VDR overexpression plasmid was transfected into fibroblasts and HT29 cells using Lipofectamine 3000 according to the manufacturer's instructions. After transfection with siRNAs or plasmid DNA for 6 h, cells were incubated for another 48 h with TGF-β1 before being harvested. Besides, in supporting part, the sequestosome 1 (p62/SQSTM1)–specific siRNAs (si p62/SQSTM1-1, 5'-GGAGTCGGATAACTGTTCA-3', si p62/SQSTM1-2, 5'-TGAGGAAGATCGCCTTGGA-3') (Ribobio) were used in fibroblasts.

Mice

Male C57BL/6 mice (6–8 weeks old) were purchased from the Nanjing Biomedical Research Institution of Nanjing University (Nanjing, China) and housed in Zhejiang Academy of Medical Sciences with a 12-h light/dark cycle in a temperature-controlled environment with regular chow and water. For the VD diet experiment, C57BL/6 mice were fed a diet containing 2000/4000 IU of VD or a VD-deficient diet after being weaned and were maintained on this diet until the end of the 9-week DSS administration (22, 53). The VD-sufficient/VD-deficient diet and the corresponding control diet were purchased from Shuyishuer Bio. Our previous study described the $VDR^{IEC\text{-}KO}$ mice (20), and the experimental mice were bred from VDR flox/flox mice crossed with intestine-specific Villin-Cre mice, while the controls were sibling littermates. All mouse experiments were approved by the Animal Care and Use Committee of the First Affiliated Hospital, College of Medicine, Zhejiang University.

Induction of DSS-induced and TNBS-induced intestinal fibrosis models

The chronic DSS-induced intestinal fibrosis model was established by three cycles of DSS administration, as described previously (54). Briefly, one cycle involved drinking DSS (MP Biomedicals) for 1 week, followed by 2 weeks of normal drinking water for recovery. This cycle was repeated three times, and the concentration of DSS was 1.5%, 2%, and 2%. For chronic TNBS administration, the mice were presensitized by the administration of 1% TNBS (Sigma-Aldrich) to the back for 1 week. As described (55), after being fasted for 24 h, the mice received 100 μl of TNBS in 50% ethanol by rectal injection with a 1-ml syringe fitted with a catheter for 6 continuous weeks. The concentrations of TNBS were 0.5%, 1.5%, 2.0%, 2.5%, 2.5%, and 2.5%. The mice were sacrificed 7 days after the last administration of TNBS. The distal colons were collected for histological analysis.

Analysis of histological scores

Paraffin-embedded sections were subjected to H&E staining for inflammation analysis and Masson's trichrome staining and Sirius red staining for fibrosis analysis. Inflammation and fibrosis scoring of mouse colon sections was performed as described previously (56). Briefly, for inflammation analysis, inflammatory cell infiltration was scored as 0 to 3, and tissue damage was scored as 0 to 3. For fibrosis analysis (11), fibrosis severity was scored as 0 to 5, ECM deposition circularity was scored as 0 to 4, and the extent of fibrosis was scored as 0 to 3. The final scoring was determined by two expert pathologists in a blinded manner.

Mouse epithelial cell isolation and dissociation

Crypt isolation was performed as described previously (57–59). Briefly, the colons were collected from $VDR^{IEC\text{-}KO}$ mice and $VDR^{fl/fl}$ mice and washed in ice-cold PBS with gentle vortexing until the luminal contents were removed. Colon tissues were digested for 20 min on ice in the dissociation reagent containing 30-mM EDTA (Sigma), 1.5-mM DTT (Sigma), and 10-μM Y27632 (Sigma). Then, the intestine was treated with another dissociation reagent (30-mM EDTA and 10-μM Y27632) and incubated at 37 °C for 10 min. The tube containing the intestine was shaken for 30 s to release the epithelium from the basement membrane. The removed epithelium was resuspended in 10 ml of Hank's Balanced Salt Solution (Sigma) containing 8 mg of dispase (Sigma) and incubated for 10 min at 37 °C. The solution was passed through 70-μm filters after the addition of 10 mg/ml DNase (Roche). After centrifugation, colonic epithelial cells were obtained.

Protein extraction and Western blotting

Protein extraction from cells or intestinal samples was performed as described previously (20). The samples were lysed with RIPA buffer (Applygen) supplemented with proteinase and phosphatase inhibitors (Sigma). A BCA protein assay kit (Applygen) was used to determine the protein concentrations. Proteins were separated by SDS-PAGE and transferred to polyvinylidene difluoride membranes (0.2-μm pore; Millipore). After being incubated in 5% nonfat milk, the membrane was incubated with primary antibodies at 4 °C overnight. Antibodies α-SMA (ab7817), fibronectin (ab2413), CTGF (ab6992), MMP9 (ab38898), TGF-β1 (ab92486), ZO-1(ab96587), occludin (ab167161), Vimentin (ab92547), ATP5A (ab14748), and SHH (ab240438) were obtained from Abcam, VDR (12550), Smad2/3 (8685), p-Smad2(3101), p-Smad3(8769), Slug (9585), E-cadherin (3195), β-catenin (8480), and GAPDH (5174) antibodies were obtained from Cell Signaling Technology, and VDAC1 antibodies were obtained from Santa Cruz (sc-390996). The p62/SQSTM1 antibodies were obtained from MBL (PM045). Then, the membrane was incubated with secondary antibodies (Sigma) at room temperature (RT) for 1 h. Proteins were detected with an ECL light detection kit (Lianke Multi Sciences). GAPDH was used as the control.

IHC and immunofluorescence staining

Paraffin-embedded sections (4-μm thick) were deparaffinized and rehydrated by serial immersion in ethanol. Then, the endogenous peroxidase activity was blocked by incubation in 3% H_2O_2 (Zsgb Bio) for 10 min, followed by antigen retrieval in citrate buffer. The sections were blocked in goat serum (Zsgb Bio) for 40 min at RT, followed by incubation with primary antibodies (VDR (CST 12550), α-SMA (ab7817), fibronectin (ab2413), and p62/SQSTM1 (PM045)) at 4 °C overnight. Then, for IHC staining, detection was performed using 3,3'-diaminobenzidine substrate (Zsgb Bio). For immunofluorescence staining, sections were incubated with DyLight 488, goat anti-mouse IgG or DyLight 594, goat anti-rabbit IgG (Abbkine) and stained with 4',6-diamidino-2-phenylindole.

RNA extraction and quantitative real-time PCR

RNA was isolated from tissue samples or cell lysates by the TRIzol (Takara) method according to the manufacturer's instructions and reverse transcribed into cDNA *via* PrimeScript RT master mix (Takara). Quantitative real-time PCR was conducted using SYBR Green (Takara Shuzo) with a Bio-Rad CFX384 system. The primer sequences are listed in Table S2. All target genes were normalized to the expression of GAPDH.

OCR

To examine the mitochondrial function of HT29 cells, we used the Agilent Seahorse XF Cell Mito Stress Test (Agilent Technologies) according to the manufacturer's instructions. The modulators included in this assay kit were oligomycin (1.5 μM), carbonyl cyanide-4 (trifluoromethoxy) phenylhydrazone (0.5 μM), and rotenone/antimycin A (0.5 μM). Each group had five replicate samples.

Measurement of serum VD levels

In the VD dietary intervention experiment, we used an AB Sciex API 3200 mass spectrometer to determine serum 25-VitD levels according to the manufacturer's instructions.

Fluorescence biodistribution

To examine the absorption efficiency of the intestinal epithelium *in vivo*, we performed a fluorescence-labeled biodistribution experiment, as described previously (60). $VDR^{IEC\text{-}KO}$ mice and $VDR^{fl/fl}$ mice were fasted overnight before the experiments. Each mouse received 200 μl of 1 mg/ml IgG-Cy5 (Nalocarry Pharmatech Ltd) by oral gavage and was sacrificed after 6 h. The colon was removed, and the colon contents were flushed with PBS. The images were taken with an IVIS Lumina II imaging system.

Transmission electron microscopy

Fresh colon tissues were collected from $VDR^{IEC\text{-}KO}$ mice and $VDR^{fl/fl}$ mice and fixed in 2.5% glutaraldehyde (Servicebio) for 4 h at RT, followed by fixation overnight at 4 °C. The preparation of electron microscopy samples and picture acquisition were performed by Servicebio Biotechnology Company (epithelial cell magnification: 7000× ; mesenchymal cell magnification: 15,000×).

Coimmunoprecipitation

As described previously (53), HEK293 cells were transfected with the FLAG–VDR plasmid. Subsequently, cells were lysed with the lysis buffer (Pierce) and then immunoprecipitated with anti-FLAG agarose (Sigma) for 3 h. After washing the immunoprecipitates, the proteins were incubated with the loading buffer and horizontally vibrated for 2 min. Finally, the supernatants were analyzed by Western blotting.

Flow cytometry

We identified isolated primary human intestinal fibroblasts by flow cytometry as described previously (51). The percentage of primary human intestinal fibroblasts gated among mesenchymal cells was greater than 95% at passage 3 (data not shown). The fluorochrome-labeled monoclonal antibodies and staining procedure were performed according to the manufacturer's protocols (BD Pharmingen). Pretreated CCD-18Co cells were stained with human anti-alpha SMA (1A4) Alexa Fluor 488 (eBioscience). The cells were analyzed with a NovoCyte flow cytometer (ACEA), and flow cytometric analysis was performed with FlowJo software.

Statistical analysis

Quantitative data are displayed as the mean ± SD. Significance testing was performed by unpaired or paired (human tissues) two-tailed Student's t tests or one-way ANOVA with Tukey's correction when appropriate. Statistical tests were performed with GraphPad Prism 8 software.

Animal and human subject statements

The study of human subject protocol abided by the Declaration of Helsinki principles and was approved by the clinical research ethics committee of the First Affiliated Hospital, College of Medicine, Zhejiang University (approval number IIT20200659A), and all mouse procedures were approved by the animal experimental ethical inspection of the First Affiliated Hospital, College of Medicine, Zhejiang University (approval number 2018-619-1).

Data availability

The authors have declared that all data are contained within the article.

Supporting information—This article contains supporting information.

Author contributions—M. Y., H. W., and J. W. proposed the initial idea, designed the study procedures, and completed most of the experiments. X. C. and Chao Lu guided the histological evaluations of inflammation. J. Z. and J. P. gathered clinical samples and data. Chunxiao Li and P. L. collected colonic tissues of mice. Y. C. and C.

T. guided the writing of the manuscript. W. Z., Q. J., and H. Z. conducted statistical analysis. J. S. and C. Y. supervised and provided consult throughout the study. All authors have read and approved the final version of this manuscript.

Funding and additional information—This work was supported and approved by Natural Science Foundation of Zhejiang Province (No. LY20H030005) and the National Natural Science Foundation of China (No. 81770547) and the Foundation of Shanghai Municipal Population and Family Planning Commission (No. 20174Y0151).

Conflict of interest—The authors declare that they have no conflicts of interest with the contents of this article.

Abbreviations—The abbreviations used are: α-SMA, alpha smooth muscle actin; CD, Crohn's disease; CTGF, connective tissue growth factor; DSS, dextran sodium sulfate; ECM, extracellular matrix; EMT, epithelial–mesenchymal transition; IHC, immunohistochemistry; MCU, mitochondrial calcium uniporter; MMP, matrix metalloproteinase; OCR, oxygen consumption rate; p62/SQSTM1, sequestosome 1; ROS, reactive oxygen species; TGF-β1, transforming growth factor-β1; TNBS, trinitrobenzene sulfonic acid; VD, vitamin D; VDAC1, voltage-dependent anion-selective channel 1; VDR, vitamin D receptor; VDR^{IEC-KO}, intestine-specific VDR-KO; ZO-1, zonulin-1.

References

1. Torres, J., Mehandru, S., Colombel, J. F., and Peyrin-Biroulet, L. (2017) Crohn's disease. *Lancet* **389**, 1741–1755
2. Thia, K. T., Sandborn, W. J., Harmsen, W. S., Zinsmeister, A. R., and Loftus, E. V., Jr. (2010) Risk factors associated with progression to intestinal complications of Crohn's disease in a population-based cohort. *Gastroenterology* **139**, 1147–1155
3. Wang, Z. T., Hu, J. J., Fan, R., Zhou, J., and Zhong, J. (2014) RAGE gene three polymorphisms with Crohn's disease susceptibility in Chinese Han population. *World J. Gastroenterol.* **20**, 2397–2402
4. Rieder, F., Zimmermann, E. M., Remzi, F. H., and Sandborn, W. J. (2013) Crohn's disease complicated by strictures: A systematic review. *Gut* **62**, 1072–1084
5. Peyrin-Biroulet, L., Loftus, E. V., Jr., Colombel, J. F., and Sandborn, W. J. (2010) The natural history of adult Crohn's disease in population-based cohorts. *Am. J. Gastroenterol.* **105**, 289–297
6. Rockey, D. C., Bell, P. D., and Hill, J. A. (2015) Fibrosis–a common pathway to organ injury and failure. *N. Engl. J. Med.* **373**, 96
7. Speca, S., Rousseaux, C., Dubuquoy, C., Rieder, F., Vetuschi, A., Sferra, R., Giusti, I., Bertin, B., Dubuquoy, L., Gaudio, E., Desreumaux, P., and Latella, G. (2016) Novel PPARgamma modulator GED-0507-34 levo ameliorates inflammation-driven intestinal fibrosis. *Inflamm. Bowel Dis.* **22**, 279–292
8. Rieder, F., Karrasch, T., Ben-Horin, S., Schirbel, A., Ehehalt, R., Wehkamp, J., de Haar, C., Velin, D., Latella, G., Scaldaferri, F., Rogler, G., Higgins, P., and Sans, M. (2012) Results of the 2nd scientific workshop of the ECCO (III): Basic mechanisms of intestinal healing. *J. Crohns Colitis* **6**, 373–385
9. Speca, S., Giusti, I., Rieder, F., and Latella, G. (2012) Cellular and molecular mechanisms of intestinal fibrosis. *World J. Gastroenterol.* **18**, 3635–3661
10. Johnson, L. A., Rodansky, E. S., Sauder, K. L., Horowitz, J. C., Mih, J. D., Tschumperlin, D. J., and Higgins, P. D. (2013) Matrix stiffness corresponding to strictured bowel induces a fibrogenic response in human colonic fibroblasts. *Inflamm. Bowel Dis.* **19**, 891–903
11. Holvoet, T., Devriese, S., Castermans, K., Boland, S., Leysen, D., Vandewynckel, Y. P., Devisscher, L., Van den Bossche, L., Van Welden, S., Dullaers, M., Vandenbroucke, R. E., De Rycke, R., Geboes, K., Bourin, A., Defert, O., *et al.* (2017) Treatment of intestinal fibrosis in experimental inflammatory bowel disease by the pleiotropic actions of a local rho kinase inhibitor. *Gastroenterology* **153**, 1054–1067
12. Scheibe, K., Backert, I., Wirtz, S., Hueber, A., Schett, G., Vieth, M., Probst, H. C., Bopp, T., Neurath, M. F., and Neufert, C. (2017) IL-36R signalling activates intestinal epithelial cells and fibroblasts and promotes mucosal healing *in vivo*. *Gut* **66**, 823–838
13. Lenti, M. V., and Di Sabatino, A. (2019) Intestinal fibrosis. *Mol. Aspects Med.* **65**, 100–109
14. Jiang, H., Shen, J., and Ran, Z. (2018) Epithelial-mesenchymal transition in Crohn's disease. *Mucosal Immunol.* **11**, 294–303
15. Scharl, M., Huber, N., Lang, S., Furst, A., Jehle, E., and Rogler, G. (2015) Hallmarks of epithelial to mesenchymal transition are detectable in Crohn's disease associated intestinal fibrosis. *Clin. Transl. Med.* **4**, 1
16. Margolis, R. N., and Christakos, S. (2010) The nuclear receptor superfamily of steroid hormones and vitamin D gene regulation. An update. *Ann. N. Y. Acad. Sci.* **1192**, 208–214
17. Christakos, S., Dhawan, P., Verstuyf, A., Verlinden, L., and Carmeliet, G. (2016) Vitamin D: Metabolism, molecular mechanism of action, and pleiotropic effects. *Physiol. Rev.* **96**, 365–408
18. He, L., Liu, T., Shi, Y., Tian, F., Hu, H., Deb, D. K., Chen, Y., Bissonnette, M., and Li, Y. C. (2018) Gut epithelial vitamin D receptor regulates microbiota-dependent mucosal inflammation by suppressing intestinal epithelial cell apoptosis. *Endocrinology* **159**, 967–979
19. Liu, W., Chen, Y., Golan, M. A., Annunziata, M. L., Du, J., Dougherty, U., Kong, J., Musch, M., Huang, Y., Pekow, J., Zheng, C., Bissonnette, M., Hanauer, S. B., and Li, Y. C. (2013) Intestinal epithelial vitamin D receptor signaling inhibits experimental colitis. *J. Clin. Invest.* **123**, 3983–3996
20. Li, C., Chen, Y., Zhu, H., Zhang, X., Han, L., Zhao, Z., Wang, J., Ning, L., Zhou, W., Lu, C., Xu, L., Sang, J., Feng, Z., Zhang, Y., Lou, X., *et al.* (2020) Inhibition of histone deacetylation by MS-275 alleviates colitis by activating the vitamin D receptor. *J. Crohns Colitis* **14**, 1103–1118
21. Gisbert-Ferrandiz, L., Cosin-Roger, J., Hernandez, C., Macias-Ceja, D. C., Ortiz-Masia, D., Salvador, P., Esplugues, J. V., Hinojosa, J., Navarro, F., Calatayud, S., and Barrachina, M. D. (2020) Diminished vitamin D receptor protein levels in Crohn's disease fibroblasts: Effects of vitamin D. *Nutrients* **12**, 973
22. Tao, Q., Wang, B., Zheng, Y., Jiang, X., Pan, Z., and Ren, J. (2015) Vitamin D prevents the intestinal fibrosis via induction of vitamin D receptor and inhibition of transforming growth factor-beta1/Smad3 pathway. *Dig. Dis. Sci.* **60**, 868–875
23. Consiglio, M., Destefanis, M., Morena, D., Foglizzo, V., Forneris, M., Pescarmona, G., and Silvagno, F. (2014) The vitamin D receptor inhibits the respiratory chain, contributing to the metabolic switch that is essential for cancer cell proliferation. *PLoS One* **9**, e115816
24. Ricca, C., Aillon, A., Bergandi, L., Alotto, D., Castagnoli, C., and Silvagno, F. (2018) Vitamin D receptor is necessary for mitochondrial function and cell health. *Int. J. Mol. Sci.* **19**, 1672
25. Chang, E. (2019) 1,25-Dihydroxyvitamin D decreases tertiary butylhydrogen peroxide-induced oxidative stress and increases AMPK/SIRT1 activation in C2C12 muscle cells. *Molecules* **24**, 3903
26. Gordon, I. O., Agrawal, N., Goldblum, J. R., Fiocchi, C., and Rieder, F. (2014) Fibrosis in ulcerative colitis: Mechanisms, features, and consequences of a neglected problem. *Inflamm. Bowel Dis.* **20**, 2198–2206
27. Ortiz-Masia, D., Salvador, P., Macias-Ceja, D. C., Gisbert-Ferrandiz, L., Esplugues, J. V., Manye, J., Alos, R., Navarro-Vicente, F., Mamie, C., Scharl, M., Cosin-Roger, J., Calatayud, S., and Barrachina, M. D. (2020) WNT2b activates epithelial-mesenchymal transition through FZD4: Relevance in penetrating Crohn s disease. *J. Crohns Colitis* **14**, 230–239
28. Ortiz-Masia, D., Gisbert-Ferrandiz, L., Bauset, C., Coll, S., Mamie, C., Scharl, M., Esplugues, J. V., Alos, R., Navarro, F., Cosin-Roger, J., Barrachina, M. D., and Calatayud, S. (2020) Succinate activates EMT in intestinal epithelial cells through SUCNR1: A novel protagonist in fistula development. *Cells* **9**, 1104
29. Duran, A., Hernandez, E. D., Reina-Campos, M., Castilla, E. A., Subramaniam, S., Raghunandan, S., Roberts, L. R., Kisseleva, T., Karin, M., Diaz-Meco, M. T., and Moscat, J. (2016) p62/SQSTM1 by binding to vitamin D receptor inhibits hepatic stellate cell activity, fibrosis, and liver cancer. *Cancer Cell* **30**, 595–609

30. Ding, N., Yu, R. T., Subramaniam, N., Sherman, M. H., Wilson, C., Rao, R., Leblanc, M., Coulter, S., He, M., Scott, C., Lau, S. L., Atkins, A. R., Barish, G. D., Gunton, J. E., Liddle, C., *et al.* (2013) A vitamin D receptor/SMAD genomic circuit gates hepatic fibrotic response. *Cell* **153**, 601–613
31. Shi, Y., Cui, X., Sun, Y., Zhao, Q., and Liu, T. (2020) Intestinal vitamin D receptor signaling ameliorates dextran sulfate sodium-induced colitis by suppressing necroptosis of intestinal epithelial cells. *FASEB J.* **34**, 13494–13506
32. Lu, X., Chen, Z., Vick, S., and Watsky, M. A. (2019) Vitamin D receptor and metabolite effects on corneal epithelial cell gap junction proteins. *Exp. Eye Res.* **187**, 107776
33. Acloque, H., Adams, M. S., Fishwick, K., Bronner-Fraser, M., and Nieto, M. A. (2009) Epithelial-mesenchymal transitions: The importance of changing cell state in development and disease. *J. Clin. Invest.* **119**, 1438–1449
34. Kemmis, C. M., and Welsh, J. (2008) Mammary epithelial cell transformation is associated with deregulation of the vitamin D pathway. *J. Cell. Biochem.* **105**, 980–988
35. Garcia, I. M., Altamirano, L., Mazzei, L., Fornes, M., Molina, M. N., Ferder, L., and Manucha, W. (2012) Role of mitochondria in paricalcitol-mediated cytoprotection during obstructive nephropathy. *Am. J. Physiol. Renal Physiol.* **302**, F1595–1605
36. Ryan, Z. C., Craig, T. A., Folmes, C. D., Wang, X., Lanza, I. R., Schaible, N. S., Salisbury, J. L., Nair, K. S., Terzic, A., Sieck, G. C., and Kumar, R. (2016) 1alpha,25-Dihydroxyvitamin D3 regulates mitochondrial oxygen consumption and dynamics in human skeletal muscle cells. *J. Biol. Chem.* **291**, 1514–1528
37. Chan, D. C. (2012) Fusion and fission: Interlinked processes critical for mitochondrial health. *Annu. Rev. Genet.* **46**, 265–287
38. Amodeo, G. F., Scorciapino, M. A., Messina, A., De Pinto, V., and Ceccarelli, M. (2014) Charged residues distribution modulates selectivity of the open state of human isoforms of the voltage dependent anion-selective channel. *PLoS One* **9**, e103879
39. Camara, A. K. S., Zhou, Y., Wen, P. C., Tajkhorshid, E., and Kwok, W. M. (2017) Mitochondrial VDAC1: A key gatekeeper as potential therapeutic target. *Front. Physiol.* **8**, 460
40. Marchi, S., and Pinton, P. (2014) The mitochondrial calcium uniporter complex: Molecular components, structure and physiopathological implications. *J. Physiol.* **592**, 829–839
41. Anand, R., Wai, T., Baker, M. J., Kladt, N., Schauss, A. C., Rugarli, E., and Langer, T. (2014) The i-AAA protease YME1L and OMA1 cleave OPA1 to balance mitochondrial fusion and fission. *J. Cell Biol.* **204**, 919–929
42. Huang, H., Shah, K., Bradbury, N. A., Li, C., and White, C. (2014) Mcl-1 promotes lung cancer cell migration by directly interacting with VDAC to increase mitochondrial Ca2+ uptake and reactive oxygen species generation. *Cell Death Dis.* **5**, e1482
43. Varanita, T., Soriano, M. E., Romanello, V., Zaglia, T., Quintana-Cabrera, R., Semenzato, M., Menabo, R., Costa, V., Civiletto, G., Pesce, P., Viscomi, C., Zeviani, M., Di Lisa, F., Mongillo, M., Sandri, M., *et al.* (2015) The OPA1-dependent mitochondrial cristae remodeling pathway controls atrophic, apoptotic, and ischemic tissue damage. *Cell Metab.* **21**, 834–844
44. Yang, L., Wu, L., Zhang, X., Hu, Y., Fan, Y., and Ma, J. (2017) 1,25(OH) 2D3/VDR attenuates high glucoseinduced epithelialmesenchymal transition in human peritoneal mesothelial cells via the TGFbeta/Smad3 pathway. *Mol. Med. Rep.* **15**, 2273–2279
45. Palmer, H. G., Gonzalez-Sancho, J. M., Espada, J., Berciano, M. T., Puig, I., Baulida, J., Quintanilla, M., Cano, A., de Herreros, A. G., Lafarga, M., and Munoz, A. (2001) Vitamin D(3) promotes the differentiation of colon carcinoma cells by the induction of E-cadherin and the inhibition of beta-catenin signaling. *J. Cell Biol.* **154**, 369–387
46. Schneider, M., Khalil, A. A., Poulton, J., Castillejo-Lopez, C., Egger-Adam, D., Wodarz, A., Deng, W. M., and Baumgartner, S. (2006) Perlecan and dystroglycan act at the basal side of the Drosophila follicular epithelium to maintain epithelial organization. *Development* **133**, 3805–3815
47. Lee, C. T., Wang, J. Y., Chou, K. Y., and Hsu, M. I. (2019) 1,25-Dihydroxyvitamin D3 modulates the effects of sublethal BPA on mitochondrial function via activating PI3K-Akt pathway and 17beta-estradiol secretion in rat granulosa cells. *J. Steroid Biochem. Mol. Biol.* **185**, 200–211
48. Chen, C., Luo, Y., Su, Y., and Teng, L. (2019) The vitamin D receptor (VDR) protects pancreatic beta cells against Forkhead box class O1 (FOXO1)-induced mitochondrial dysfunction and cell apoptosis. *Biomed. Pharmacother.* **117**, 109170
49. Lisse, T. S., Saini, V., Zhao, H., Luderer, H. F., Gori, F., and Demay, M. B. (2014) The vitamin D receptor is required for activation of cWnt and Hedgehog signaling in keratinocytes. *Mol. Endocrinol.* **28**, 1698–1706
50. Bikle, D. D., Oda, Y., Tu, C. L., and Jiang, Y. (2015) Novel mechanisms for the vitamin D receptor (VDR) in the skin and in skin cancer. *J. Steroid Biochem. Mol. Biol.* **148**, 47–51
51. Scheibe, K., Kersten, C., Schmied, A., Vieth, M., Primbs, T., Carle, B., Knieling, F., Claussen, J., Klimowicz, A. C., Zheng, J., Baum, P., Meyer, S., Schurmann, S., Friedrich, O., Waldner, M. J., *et al.* (2019) Inhibiting interleukin 36 receptor signaling reduces fibrosis in mice with chronic intestinal inflammation. *Gastroenterology* **156**, 1082–1097.e1011
52. Honzawa, Y., Nakase, H., Shiokawa, M., Yoshino, T., Imaeda, H., Matsuura, M., Kodama, Y., Ikeuchi, H., Andoh, A., Sakai, Y., Nagata, K., and Chiba, T. (2014) Involvement of interleukin-17A-induced expression of heat shock protein 47 in intestinal fibrosis in Crohn's disease. *Gut* **63**, 1902–1912
53. Zhang, H., Shen, Z., Lin, Y., Zhang, J., Zhang, Y., Liu, P., Zeng, H., Yu, M., Chen, X., Ning, L., Mao, X., Cen, L., Yu, C., and Xu, C. (2020) Vitamin D receptor targets hepatocyte nuclear factor 4alpha and mediates protective effects of vitamin D in nonalcoholic fatty liver disease. *J. Biol. Chem.* **295**, 3891–3905
54. Breynaert, C., de Bruyn, M., Arijs, I., Cremer, J., Martens, E., Van Lommel, L., Geboes, K., De Hertogh, G., Schuit, F., Ferrante, M., Vermeire, S., Ceuppens, J., Opdenakker, G., and Van Assche, G. (2016) Genetic deletion of tissue inhibitor of metalloproteinase-1/TIMP-1 alters inflammation and attenuates fibrosis in dextran sodium sulphate-induced murine models of Colitis. *J. Crohns Colitis* **10**, 1336–1350
55. Wirtz, S., Popp, V., Kindermann, M., Gerlach, K., Weigmann, B., Fichtner-Feigl, S., and Neurath, M. F. (2017) Chemically induced mouse models of acute and chronic intestinal inflammation. *Nat. Protoc.* **12**, 1295–1309
56. Zhang, J., Xu, M., Zhou, W., Li, D., Zhang, H., Chen, Y., Ning, L., Zhang, Y., Li, S., Yu, M., Chen, Y., Zeng, H., Cen, L., Zhou, T., Zhou, X., *et al.* (2020) Deficiency in the anti-apoptotic protein DJ-1 promotes intestinal epithelial cell apoptosis and aggravates inflammatory bowel disease via p53. *J. Biol. Chem.* **295**, 4237–4251
57. Nanki, K., Fujii, M., Shimokawa, M., Matano, M., Nishikori, S., Date, S., Takano, A., Toshimitsu, K., Ohta, Y., Takahashi, S., Sugimoto, S., Ishimaru, K., Kawasaki, K., Nagai, Y., Ishii, R., *et al.* (2020) Somatic inflammatory gene mutations in human ulcerative colitis epithelium. *Nature* **577**, 254–259
58. Gjorevski, N., Sachs, N., Manfrin, A., Giger, S., Bragina, M. E., Ordonez-Moran, P., Clevers, H., and Lutolf, M. P. (2016) Designer matrices for intestinal stem cell and organoid culture. *Nature* **539**, 560–564
59. Gracz, A. D., Puthoff, B. J., and Magness, S. T. (2012) Identification, isolation, and culture of intestinal epithelial stem cells from murine intestine. *Methods Mol. Biol.* **879**, 89–107
60. Liu, D., Jin, F., Shu, G., Xu, X., Qi, J., Kang, X., Yu, H., Lu, K., Jiang, S., Han, F., You, J., Du, Y., and Ji, J. (2019) Enhanced efficiency of mitochondria-targeted peptide SS-31 for acute kidney injury by pH-responsive and AKI-kidney targeted nanopolyplexes. *Biomaterials* **211**, 57–67